Evaporation-Induced Liquid Expansion and Bubble Formation in Binary Mixtures

Qiyun Tang[*] and Marcus Müller[†]
Institut für Theoretische Physik, Universität Göttingen, Friedrich-Hund-Platz 1, 37077 Göttingen, Germany

(Received 13 October 2020; accepted 18 December 2020; published 13 January 2021)

We observe an anomalous liquid expansion after quenching a binary mixture at coexistence to low pressures in the vapor phase by numerical calculations. This evaporation-induced expansion can be attributed to the pressure imbalance near the liquid-vapor interface, which originates from the interplay between the complex thermodynamics of binary mixtures both in the vapor and liquid phases, as well as their dynamical asymmetries. In addition, careful modulation of the pressure quench in the vapor phase can result in spinodal bubble formation inside liquid phase. The results indicate that the thermodynamics-kinetics interplay could foster our fundamental understanding of the evaporation process and promote its practical applications.

DOI: 10.1103/PhysRevLett.126.028003

Solvent evaporation is a physical process underlying the fabrication of soft-matter films via common techniques such as dip coating or spin coating onto a substrate [1–3]. The evaporation of solvents induces a pressure drop inside the liquid phase, which gradually shrinks and concentrates the nonvolatile component (solute) of the soft-matter solutions, often giving rise to the formation of nano- and mesostructures [4–7]. Such a physical process has been widely applied to guide the self-assembly of soft-matter films, such as polymer-based nanostructures [8–18], micelles [19], 2D crystals [20,21], colloids films [3,6, 22–24], as well as silica-based [1,25] or transition-metal-based (such as titanium dioxide, TiO_2) [26–35] mesoporous thin films. Conversely, vapor-annealing approaches have been employed to swell less-ordered nanostructures through higher vapor pressures to facilitate the rearrangement toward well-ordered, thermodynamic equilibrium structures [15,36,37]. The theoretical understanding of the evaporation process chiefly focuses on the spatiotemporal evolution of solvents or solutes inside the liquid film by solving the diffusion equations [23,38–44], often supplemented by a "moving boundary condition" [44–47] to characterize the recession of the free surface. However, the role of solvent thermodynamics in the vapor phase in evaporation has been rarely explored.

Recently, binary mixtures of solvents have been employed to tailor the structure and thermodynamics of soft materials [48–55]. Binary solvents are especially important for the fabrication of transition-metal mesoporous thin films via evaporation induced self-assembly (EISA) [26–35]. For example, hydrogen chloride (HCl) and water are commonly employed for the formation of titanium dioxide mesoporous structures [26–30] because the acid HCl can efficiently inhibit the high reactivity of titanium precursors [56], whereas water tailors the interactions between surfactants and precursors [27]. The binary mixture of water and HCl forms a negative azeotrope [57–60], i.e., there exist thermodynamic conditions such that the coexisting liquid and vapor phases have identical relative composition. This behavior indicates the strong association between water and HCl molecules. Such complex thermodynamics of binary solvents will make the evaporation process significantly different from that of a single solvent and the thermodynamics in the vapor phase cannot be accurately approximated by that of an ideal gas. The evolution of the liquid phase in the course of evaporation depends on the thermodynamics of the liquid mixtures and the exchange with the vapor phase across the liquid-vapor interface. Because of the nontrivial densities inside the vapor phase at high pressures, the thermodynamics of the one-component vapor phase can be qualitatively captured by the phenomenological mean-field theories [61]. To the best of our knowledge, there has been no investigation of the interplay between the thermodynamics and kinetics in the liquid and vapor phases and the consequences for the spatiotemporal evolution in the course of evaporation from binary solvents.

In this Letter, we suddenly drop the pressure in the vapor phase of a negative azeotrope and observe an anomalous evaporation-induced liquid expansion at suitable conditions. This liquid expansion can be attributed to the pressure imbalance across the liquid-vapor interface, which originates from the interplay between the complex thermodynamics of binary mixtures both in the vapor and liquid phases, as well as their dynamical asymmetries. We also demonstrate that a one-step strong pressure quench in the vapor phase can drive the liquid, originally coexisting with its vapor, across the spinodal line into the unstable region, resulting in the spontaneous formation of bubbles, whereas a multiple small-step quench can avoid bubble formation. Our findings exemplify that the interplay of thermodynamics and kinetics in binary solvent mixtures offer

ample opportunities to control evaporation-induced structure formation and provide a simple, general theoretical framework for exploring these effects.

We describe the thermodynamics of a compressible, binary mixture by a phenomenological free-energy density in terms of segment densities, ϕ_A and ϕ_B, and keep interaction terms up to third order [62–66]:

$$\frac{f_{\rm hom}}{k_BT} = \sum_{i=A,B}\frac{\phi_i}{N_i}\left(\ln\frac{\phi_i}{N_i}-1\right)+\frac{v_{AA}}{2}\phi_A^2 + v_{AB}\phi_A\phi_B+\frac{v_{BB}}{2}\phi_B^2+\frac{w_{AAA}}{3}\phi_A^3 + w_{AAB}\phi_A^2\phi_B+w_{ABB}\phi_A\phi_B^2+\frac{w_{BBB}}{3}\phi_B^3. \quad (1)$$

The first terms are the entropy of mixing. v_{AA}, v_{AB}, and v_{BB} describe the pairwise interactions between A and B segments. The coefficients w_{AAA}, w_{AAB}, w_{ABB}, and w_{BBB}, in turn, characterize triple interactions. In the low-density limit this expression corresponds to the virial expansion but conceiving the coefficients as effective parameters significantly enlarges the range of validity [62–66]. For our calculations, we choose $v_{AA}=-3.30$, $v_{AB}=-3.14$ and $v_{BB}=-6.42$, $w_{AAA}=2.93$, $w_{AAB}=2.69$, $w_{ABB}=1.60$, $w_{BBB}=4.00$, and $N_A=2$ and $N_B=1$. The phase diagram of the binary mixture as a function of pressure and density fraction of the A component, $f_A=\phi_A/(\phi_A+\phi_B)$, can be calculated from Eq. (1); see details in the Supplemental Material [67]. Figure 1(a) shows the phase diagram of a negative azeotrope, which qualitatively describes the phase behavior of water and acids of low molecular weights.

In order to describe a spatially inhomogeneous system, we add square gradient terms to the free-energy functional [68]

$$\frac{\mathcal{F}[\phi_A,\phi_B]}{k_BT}=\int d\mathbf{r}\left(\frac{f_{\rm hom}}{k_BT}+\frac{\gamma_A}{2}|\nabla\phi_A|^2+\frac{\gamma_B}{2}|\nabla\phi_B|^2\right), \quad (2)$$

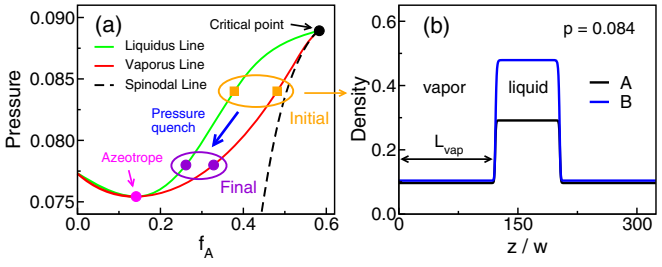

FIG. 1. (a) Equilibrium phase diagram of negative azeotrope mixture. The blue arrow illustrates the pressure quench from the dimensionless initial pressure $p_{\rm init}=0.084$ (orange) to $p_{\rm final}=0.078$ (violet). (b) Liquid-vapor phase coexistence at $p_{\rm init}=0.084$. The phase coexistence is marked in panel (a), providing the density fraction of A in the coexisting liquid and vapor phases.

where γ_A and γ_B characterize the square width of the liquid-vapor interface. We choose $\gamma_A=\gamma_B=0.01$. Figure 1(b) shows the profile of the interface between the coexisting phases, liquid and vapor, at pressure $p=0.084$.

Given the free-energy functional, we use the locally conserved diffusion equations [69] to describe the time evolution of the densities:

$$\frac{\partial\phi_i}{\partial t}=D_i\nabla^2\frac{\delta\mathcal{F}}{\delta\phi_i} \quad \text{for } i=A,B, \quad (3)$$

here D_A and D_B are the diffusion coefficients of A and B species, which are taken to be density independent [70,71]. We solve Eq. (3) in one dimension, z, within a box of length $L_z=324w$ using the Dirichlet boundary conditions, and w is the width of the liquid-vapor interface at $p=0.084$, see Supplemental Material [67]. We rescale the time $t'=t/\tau$ (we still use t to replace t' in the following discussions), where $\tau=100w^2/D_B$ characterizes the time to cross a length of 10 liquid-vapor interfaces for B species. In addition, we choose $\alpha=D_A/D_B$ to characterize the dynamical asymmetry between A and B species.

We conceive evaporation as a pressure quench, $p_{\rm init}=0.084$ to $p_{\rm final}=0.078$, that alters the densities of A and B a distance $L_{\rm vap}$ away from the liquid-vapor interface of the film (see Fig. 1). The boundary values are chosen to be the coexisting densities at the final pressure. The time evolution of A and B densities at $\alpha=1.0$ is shown in Figs. 2(a) and 2(c). One observes that the A density in the vapor phase gradually decreases, giving rise to the evaporation of A species through the vapor phase. Such an evaporation drives the A density toward its new, smaller coexistence density at the lower $p_{\rm final}$. The positive B flux through the vapor phase increases the B density in the liquid phase, see Fig. 2(c). This can be attributed to the higher chemical potential of B species at its lower density in the vapor phase, see Fig. S4(b). We also observe the formation of a skin layer of B species in the liquid phase at the moving liquid-vapor interface, which has been previously predicted by theory [38–42] and simulations [21,47,65,72,73]. The liquid-vapor interfaces in Figs. 2(a) and 2(c) move toward the interior of liquid phase, indicating the shrinking of film thickness. Such evaporation-induced film shrinkage has been extensively studied [1–7], and can be attributed to the pressure drop inside the liquid due to the evaporation flux of solvents [4–7]. We also calculate the pressure evolution in both, liquid and vapor phases, where a pressure drop inside the liquid phase is observed, see Fig. 2(e) [74]. This pressure drop drives the liquid-vapor interface toward the interior of liquid film.

If we decrease the dynamical asymmetry to $\alpha=0.1$, such that the A species diffuse slower than B, the densities of A and B in the liquid and vapor phases eventually also approach their coexistence values on $p_{\rm final}=0.078$

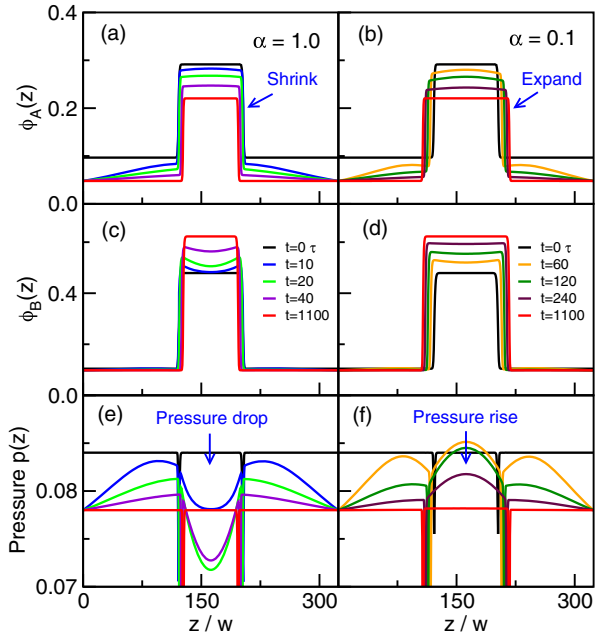

FIG. 2. (a)–(b) Time evolution of A density after a pressure quench, $p = 0.084 \rightarrow 0.078$, at the boundary for (a) $\alpha = 1.0$ and (b) $\alpha = 0.1$. (c)–(d) The time evolution of B density. (e)–(f) The variation of pressure along the z axis.

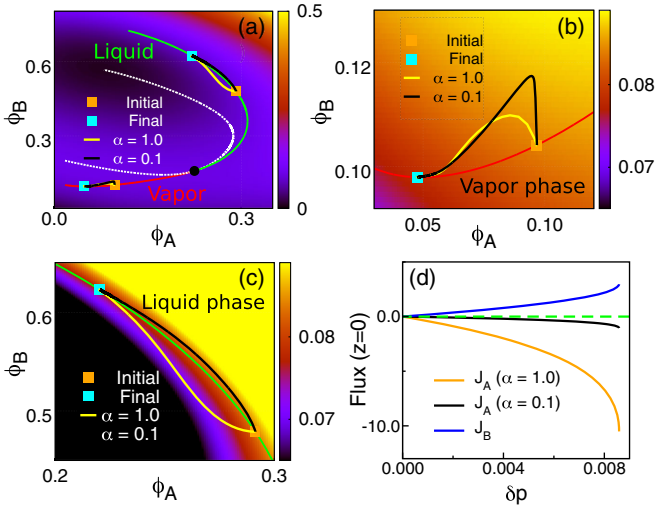

FIG. 3. (a) Contour plot of bulk pressure as a function of A and B densities, ϕ_A and ϕ_B. The red and green lines show the coexistence densities, whereas the dashed white line represents the spinodal line. The black circle shows the critical point, the orange and cyan squares depict the initial and final points in the vapor and liquid phases, respectively. The black and yellow lines show the trajectories during pressure quench for dynamical asymmetries, $\alpha = 0.1$ and 1.0. (b)–(c) Evolution of $\phi_A(z)$ and $\phi_B(z)$ in the (b) vapor ($z = 54w$) and (c) liquid ($z = 162w$) phases during the pressure quench. (d) The initial flux of A (with $\alpha = 1.0$ and 0.1, see Supplemental Material [67]) and B species at the boundary $z = 0$ after the pressure quench δp. Dashed green line shows the zero flux.

[Figs. 2(b) and 2(d)]. The movement of the liquid-vapor interfaces, however, is reversed, i.e., the liquid film expands. This anomalous expansion can be explained as follows: the decrease of A density in the liquid induced by pressure quench can be chiefly realized by the expansion of the liquid volume rather than the smaller A flux across the vapor phase (compared to B) at $\alpha = 0.1$ [Figs. S3(b) and S3(d) in Ref. [67]]. We note that the equilibrium states for distinct α in an open system have the same grand-canonical free energy and the kinetics of evaporation *selects* the final film thickness, see Supplemental Material [67]. In addition, this anomalous liquid expansion indicates that the pressure inside the liquid should be larger than that in the vapor phase. The evolution of pressure in Fig. 2(f) indeed shows a pressure rise in the liquid phase. Even in the vapor phase the pressure rises but the pressure difference across the liquid-vapor interface is positive at $\alpha = 0.1$ during most stages of the evaporation process, see Fig. S5(b) [67]. Such a reversed pressure imbalance across the interface, which originates from the pressure rise in the liquid phase, drives the interface toward the vapor region, giving rise to the anomalous liquid expansion. It is interesting to see that the liquid expansion and pressure rise are also observed transiently at small α during pressure quench in the canonical ensemble; see Supplemental Material [67]. This evaporation-induced liquid expansion could be beneficial for the rearrangement of soft materials toward well-ordered nanostructures via the evaporation-induced self-assembly [26–35].

To identify the reason for the significantly different evolutions of pressure in the liquid phase upon varying α, we present in Fig. 3(a) a contour plot of the bulk pressure as a function of ϕ_A and ϕ_B. In this graph, the coexisting densities of A and B in the liquid (top-right corner) and vapor (bottom-left corner) phases form two lines. During the evaporation, both the liquid and vapor phases will evolve from the initial, high pressure $p_{\text{init}} = 0.084$ to the lower, final pressure $p_{\text{final}} = 0.078$, forming complex trajectories in this $\phi_A - \phi_B$ plane. Here we track the density evolution at two positions, located in the vapor region, $z = 54w$, and the liquid film, $z = 162w$. Figures 3(b) and 3(c) present enlarged views of the vapor and liquid phases, respectively. In the vapor, both densities decrease upon reducing the pressure. In the liquid phase, however, the density of A decreases (thermodynamically volatile component) whereas the B density increases.

The evolution of A and B densities from $p_{\text{init}} = 0.084$ to $p_{\text{final}} = 0.078$ in the vapor phase is detailed in Fig. 3(b). For both values of α, Fig. 3(b) shows that B density and pressure in the vapor phase are always larger than the coexistence values in the course of evaporation and attain their coexistence values only at $t = 0$ or $t \rightarrow \infty$. Such trajectories are chiefly dictated by the initial flux of A and B species right after the pressure quench at the boundary $z = 0$, see Fig. 3(d). The positive B and negative A fluxes in Fig. 3(d) are determined by their complex chemical potentials, see Fig. S4 in Supplemental Material [67].

At $\alpha = 1.0$, the magnitudes of initial A and B fluxes are comparable, driving the trajectory toward the top-left orientation in Fig. 3(b) near the initial point. For $\alpha = 0.1$, the smaller A flux turns the trajectory toward the vertical orientation after leaving the initial point.

The behavior in the liquid phase, presented in Fig. 3(c), qualitatively depends on the dynamical asymmetry, α. For $\alpha = 1.0$, the comparable A and B fluxes drive the pressure below the coexistence curve, therefore the pressure is smaller than that in the vapor, resulting in film shrinking. For $\alpha = 0.1$, however, the smaller A flux rises the pressure in the liquid above the coexistence pressure and, for most times, also the pressure in the vapor, cf. Fig. S5(b). This results in an expansion of the liquid film. Such distinctions are dictated by the interplay between the complex thermodynamics of binary mixtures and their dynamical asymmetries. The dynamical asymmetry of binary solvents can be modified by choosing the solvents with different sizes, such as water and organic acids of distinct molecular weights [75] or temperature-dependent interactions, such as hydrogen bonds. It is worth noting that the pressure deviations inside the liquid film at different system sizes (with the same ratio of the liquid and vapor lengths) can be collapsed onto one master curve, see Fig. S8(b) [67], therefore we expect our findings to be valid for large, even macroscopic systems. In addition, hydrodynamic effects [69,76–78] can only influence the magnitudes of the pressure variations inside liquid phase, but they cannot alter the sign of the pressure variation, see Supplemental Material [67].

The pressure drop in Fig. 2(e) can approach the values smaller than the final pressure, see the evolution of liquid at $z = 162w$ in Fig. 4(a) (blue curve). This trend indicates that the pressure drop might drive the liquid phase across the spinodal line into unstable regions if the initial pressure goes closer to the critical point. Figure 4(b) shows the evolution of the two-dimensional A density, $\phi_A(x, z)$, after quenching the pressure from $p = 0.088$ to 0.078 at the boundary [79]. One can see that the liquid phase becomes unstable and spontaneously forms bubbles inside the liquid. We plot the evolution of liquid ($5.4w$, $108.1w$) and bubble ($5.4w$, $124.3w$) on the phase diagram in Fig. 4(a), one can see that the pressure in the liquid phase indeed passes across the spinodal line, subsequently the two points evolve to densities of liquid and vapor coexisting at $p_{\text{final}} = 0.078$. The evolution on the $p(\phi_A - \phi_B)$ plane in Fig. 4(c) clearly shows the splitting of the trajectory into distinct portions after crossing the spinodal line: one being similar to the density evolution in the liquid whereas the other portion generates bubbles inside the liquid via spinodal decomposition. Experiments have demonstrated that the evaporation of binary solvents could fabricate hierarchical mesopores [80,81], whereas the big pores of a well-defined size indicate a characteristic length scale associated with

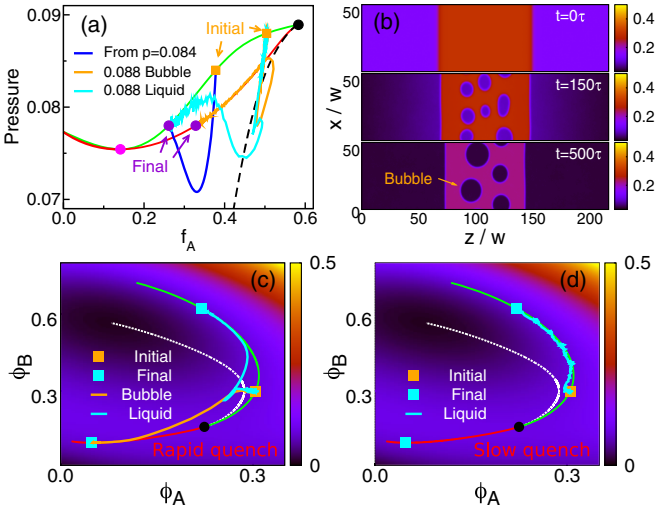

FIG. 4. (a) Equilibrium phase diagram of the binary mixtures with the same labels as Fig. 1(a). The blue line shows the evolution of liquid from $p = 0.084$ to 0.078 as in Fig. 2(e) ($z = 162w$). The orange and cyan curves show the trajectories inside a bubble ($5.4w$, $124.3w$) and the liquid ($5.4w$, $108.1w$) within the 2D film; see panel (b). (b) Time evolution of two-dimensional A density, $\phi_A(x, z)$, from $p = 0.088$ to 0.078 at $\alpha = 1.0$ with $t = 0$, 150, and 500τ. (c) Trajectories of the densities inside a bubble and the liquid on the $\phi_A - \phi_B$ plane after a rapid one-step quench. (d) Same as (c) (for the liquid) after a slow, continuous quench (multiple small-step quench).

the unstable, fastest growing density fluctuations [82]. These experimental observations are consistent with our predictions of bubble formation via the spinodal decomposition of binary solvents. It is interesting to predict that one can avoid the bubble formation inside the liquid phase by simply quenching the vapor pressure slowly, via a multiple small-step quench (from $p = 0.088 \to 0.086 \to 0.084 \to 0.082 \to 0.080 \to 0.078$), rather than the rapid one-step quench (from $p = 0.088 \to 0.078$ directly) of the vapor phase. Figure 4(d) shows that the multiple small-step quench indeed avoids crossing the spinodal, and the liquid smoothly evolves toward its new coexistence at p_{final}.

Evaporation is a physical process where the solvents diffuse from the interface of soft matter solutions [1–3], which recedes the interfaces due to the pressure drop inside the liquid phase [4–7]. This evaporation-induced recession, however, can be altered toward liquid expansion during the evaporation of binary solvents with distinct diffusion coefficients because of the interplay between their complex thermodynamics in both, the vapor and liquid phases, and dynamical asymmetries, see Figs. 3(b) and 3(c). This evaporation-induced expansion could be beneficial for the rearrangement of soft materials toward well-ordered nanostructures via the evaporation-induced self-assembly. We also demonstrate that the careful modulation of the pressure quench in the vapor phase could tailor bubble

formation inside the liquid phase. The results imply that the interplay of thermodynamics and kinetics could promote fundamental understandings of the evaporation process and its practical applications. We foresee that these findings could also stimulate the explorations of thermodynamics-kinetics interplay on other nonequilibrium process.

The authors acknowledge the financial support from the Deutsche Forschungsgemeinschaft under Grant No. Mu1674/15-2. The numerical calculations have been performed at the GWDG Göttingen, the HLRN Göttingen, and the von-Neumann Institute for Computing, Jülich, Germany.

*qiyun.tang@theorie.physik.uni-goettingen.de
†mmueller@theorie.physik.uni-goettingen.de

[1] C. J. Brinker, Y. Lu, A. Sellinger, and H. Fan, Adv. Mater. **11**, 579 (1999).
[2] A. F. Routh, Rep. Prog. Phys. **76**, 046603 (2013).
[3] J. Zhou, X. Man, Y. Jiang, and M. Doi, Adv. Mater. **29**, 1703769 (2017).
[4] L. R. White, J. Colloid Interface Sci. **90**, 536 (1982).
[5] A. F. Routh and W. B. Russel, Langmuir **15**, 7762 (1999).
[6] J. M. Salamanca, E. Ciampi, D. A. Faux, P. M. Glover, P. J. McDonald, A. F. Routh, A. C. I. A. Peters, R. Satguru, and J. L. Keddie, Langmuir **17**, 3202 (2001).
[7] S. Arai and M. Doi, Eur. Phys. J. E **35**, 57 (2012).
[8] K. E. Strawhecker, S. K. Kumar, J. F. Douglas, and A. Karim, Macromolecules **34**, 4669 (2001).
[9] E. Ciampi and P. J. McDonald, Macromolecules **36**, 8398 (2003).
[10] L. Pauchard and C. Allain, Europhys. Lett. **62**, 897 (2003).
[11] S. H. Kim, M. J. Misner, and T. P. Russell, Adv. Mater. **16**, 2119 (2004).
[12] S. H. Kim, M. J. Misner, T. Xu, M. Kimura, and T. P. Russell, Adv. Mater. **16**, 226 (2004).
[13] Y. Shimokawa, T. Kajiya, K. Sakai, and M. Doi, Phys. Rev. E **84**, 051803 (2011).
[14] W. A. Phillip, M. A. Hillmyer, and E. L. Cussler, Macromolecules **43**, 7763 (2010).
[15] C. Sinturel, M. Vayer, M. Morris, and M. A. Hillmyer, Macromolecules **46**, 5399 (2013).
[16] C. Stegelmeier, A. Exner, S. Hauschild, V. Filiz, J. Perlich, S. V. Roth, V. Abetz, and S. Förster, Macromolecules **48**, 1524 (2015).
[17] J. Hao, Z. Wang, Z. Wang, Y. Yin, R. Jiang, B. Li, and Q. Wang, Macromolecules **50**, 4384 (2017).
[18] J. Cummings, J. S. Lowengrub, B. G. Sumpter, S. M. Wise, and R. Kumar, Soft Matter **14**, 1833 (2018).
[19] X. Ma, Y. Xia, E. qiang Chen, Y. Mi, X. Wang, and A. C. Shi, Langmuir **20**, 9520 (2004).
[20] H. Qi, W. Wang, and C. Y. Li, ACS Macro Lett. **3**, 675 (2014).
[21] Q. Tang, M. Müller, C. Y. Li, and W. Hu, Phys. Rev. Lett. **123**, 207801 (2019).
[22] S. Cheng and G. S. Grest, J. Chem. Phys. **138**, 064701 (2013).
[23] J. Zhou, Y. Jiang, and M. Doi, Phys. Rev. Lett. **118**, 108002 (2017).
[24] S. Cheng and G. S. Grest, ACS Macro Lett. **5**, 694 (2016).
[25] F. Cagnol, D. Grosso, G. J. de A. A. Soler-Illia, E. L. Crepaldi, F. Babonneau, H. Amenitsch, and C. Sanchez, J. Mater. Chem. **13**, 61 (2003).
[26] E. L. Crepaldi, G. J. de A. A. Soler-Illia, D. Grosso, F. Cagnol, F. Ribot, and C. Sanchez, J. Am. Chem. Soc. **125**, 9770 (2003).
[27] G. J. de A. A. Soler-Illia, E. Scolan, A. Louis, P. A. Albouy, and C. Sanchez, New J. Chem. **25**, 156 (2001).
[28] G. J. de A. A. Soler-Illia and C. Sanchez, New J. Chem. **24**, 493 (2000).
[29] G. J. de A. A. Soler-Illia, P. C. Angelome, M. C. Fuertes, D. Grosso, and C. Boissiere, Nanoscale **4**, 2549 (2012).
[30] Q. Tang, P. C. Angelome, G. J. A. A. Soler-Illia, and M. Müller, Phys. Chem. Chem. Phys. **19**, 28249 (2017).
[31] D. Grosso, C. Boissière, B. Smarsly, T. Brezesinski, N. Pinna, P. A. Albouy, H. Amenitsch, M. Antonietti, and C. Sanchez, Nat. Mater. **3**, 787 (2004).
[32] M. J. Henderson, A. Gibaud, J. F. Bardeau, and J. W. White, J. Mater. Chem. **16**, 2478 (2006).
[33] W. Li, Z. Wu, J. Wang, A. A. Elzatahry, and D. Zhao, Chem. Mater. **26**, 287 (2014).
[34] A. Zelcer and G. J. A. A. Soler-Illia, J. Mater. Chem. C **1**, 1359 (2013).
[35] N. Tarutani, Y. Tokudome, M. Jobbagy, G. J. A. A. Soler-Illia, Q. Tang, M. Müller, and M. Takahashi, Chem. Mater. **31**, 322 (2019).
[36] S.-M. Hur, G. Khaira, A. Ramirez-Hernandez, M. Müller, P. Nealey, and J. J. de Pablo, ACS Macro Lett. **4**, 11 (2015).
[37] X. Xu, X. Man, M. Doi, Z. C Ou-yang, and D. Andelman, Macromolecules **52**, 9321 (2019).
[38] D. E. Bornside, C. W. Macosko, and L. E. Scriven, J. Appl. Phys. **66**, 5185 (1989).
[39] P. G. de Gennes, Eur. Phys. J. E **7**, 31 (2002).
[40] T. Okuzono, K. Ozawa, and M. Doi, Phys. Rev. Lett. **97**, 136103 (2006).
[41] K. Ozawa, T. Okuzono, and M. Doi, Jap. J. Appl. Phys. **45**, 8817 (2006).
[42] A. Münch, C. P. Please, and B. Wagner, Phys. Fluids **23**, 102101 (2011).
[43] S. P. Paradiso, K. T. Delaney, C. J. García-Cervera, H. D. Ceniceros, and G. H. Fredrickson, ACS Macro Lett. **3**, 16 (2014).
[44] X. Man and M. Doi, Phys. Rev. Lett. **116**, 066101 (2016).
[45] J. Crank, *Mathematics of Diffusion* (Oxford University Press, Oxford, 1975).
[46] J. Crank, *Free and Moving Boundary Problems* (Clarendon Press, Oxford, 1984).
[47] S. Peter, H. Meyer, and J. Baschnagel, J. Chem. Phys. **131**, 014903 (2009).
[48] V. Abetz, T. Brinkmann, M. Dijkstra, K. Ebert, D. Fritsch, K. Ohlrogge, D. Paul, K.-V. Peinemann, S. P. Nunes, N. Scharnagl, and M. Schossig, Adv. Eng. Mater. **8**, 328 (2006).
[49] V. Abetz, Macromol. Rapid Commun. **36**, 10 (2015).
[50] D. R. Tree, K. T. Delaney, H. D. Ceniceros, T. Iwama, and G. H. Fredrickson, Soft Matter **13**, 3013 (2017).

[51] D. R. Tree, T. Iwama, K. T. Delaney, J. Lee, and G. H. Fredrickson, ACS Macro Lett. **7**, 582 (2018).
[52] D. Mukherji, C. M. Marques, T. Stuehn, and K. Kremer, Nat. Commun. **8**, 1374 (2017).
[53] D. Mukherji, M. D. Watson, S. Morsbach, M. Schmutz, M. Wagner, C. M. Marques, and K. Kremer, Macromolecules **52**, 3471 (2019).
[54] D. Mukherji, C. M. Marques, and K. Kremer, Annu. Rev. Condens. Matter Phys. **11**, 271 (2020).
[55] Y. Zhao, M. K. Singh, K. Kremer, R. Cortes-Huerto, and D. Mukherji, Macromolecules **53**, 2101 (2020).
[56] J. Livage, M. Henry, and C. Sanchez, Prog. Solid State Chem. **18**, 259 (1988).
[57] J. T. F. Kao, J. Chem. Eng. Data **15**, 362 (1970).
[58] P. Wang, A. Anderko, and R. D. Young, Fluid Phase Equilib. **203**, 141 (2002).
[59] B. T. Brandes, Ind. Eng. Chem. Res. **44**, 639 (2005).
[60] R. Iannarelli and M. J. Rossi, Atmos. Chem. Phys. **14**, 5183 (2014).
[61] M. J. Stott and W. H. Young, Phys. Chem. Liq. **11**, 95 (1981).
[62] P. H. V. Konynenburg and R. L. Scott, Phil. Trans. R. Soc. A **298**, 495 (1980).
[63] M. Müller, L. G. MacDowell, P. Virnau, and K. Binder, J. Chem. Phys. **117**, 5480 (2002).
[64] M. Müller, Phys. Rev. E **65**, 030802(R) (2002).
[65] M. Müller and G. D. Smith, J. Polym. Sci. B **43**, 934 (2005).
[66] K. Binder, M. Müller, P. Virnau, and L. G. MacDowell, Adv. Polym. Sci. **173**, 1 (2005).
[67] See Supplemental Material at http://link.aps.org/supplemental/10.1103/PhysRevLett.126.028003 for the phase-diagram calculation of binary negative azeotropes; the pressure, chemical potential, and flux profiles of coexisting binary mixtures; the pressure difference across liquid-vapor interface; the influence of liquid and vapor lengths, as well as hydrodynamic effects on the pressure evolution in the liquid phase; evaporation in the canonical ensemble; and influence of dynamic asymmetry on the interface movement.
[68] J. W. Cahn and J. E. Hilliard, J. Chem. Phys. **28**, 258 (1958).
[69] P. C. Hohenberg and B. I. Halperin, Rev. Mod. Phys. **49**, 435 (1977).
[70] A general diffusion equation can be written as $\partial\phi_i/\partial t = \nabla[D_i\phi_i\nabla(\delta\mathcal{F}/\delta\phi_i)]$, where $i = A, B$. In most cases, the self-diffusion coefficient D_i becomes smaller as ϕ_i increases [71], therefore one could choose a simple approximation: $D_i = D_{i0}/\phi_i$, here D_{i0} represents the self-diffusion coefficient in the melt, or at a reference density, therefore it is independent from density ϕ_i. After substituting D_i to the general diffusion equation, we obtain Fig. (3), where we still use D_i to replace D_{i0}.
[71] U. Zettl, S. T. Hoffmann, F. Koberling, G. Krausch, J. Enderlein, L. Harnau, and M. Ballauff, Macromolecules **42**, 9537 (2009).
[72] M. Tsige and G. S. Grest, Macromolecules **37**, 4333 (2004).
[73] M. Tsige and G. S. Grest, J. Phys. Condens. Matter **17**, S4119 (2005).
[74] The rapid pressure variation across the liquid-vapor interface stems from the interface tension and is irrelevant to the discussion.
[75] H. Tanaka, J. Phys. Condens. Matter **12**, R207 (2000).
[76] B. I. Halperin, P. C. Hohenberg, and E. D. Siggia, Phys. Rev. Lett. **32**, 1289 (1974).
[77] K. Kawasaki, T. Koga, and T. Kawakatsu, Mater. Res. Soc. Symp. Proc. **237**, 87 (1991).
[78] N. M. Maurits, A. V. Zvelindovsky, G. J. A. Sevink, B. A. C. van Vlimmeren, and J. G. E. M. Fraaije, J. Chem. Phys. **108**, 9150 (1998).
[79] Here we add small fluctuations with the magnitude of around 10^{-4} to A and B densities during the evaporation. These small fluctuations do not influence the thermodynamics and kinetic of the system, but are necessary to induce an isotropic spinodal decomposition at early stages when the system becomes unstable.
[80] L. Malfatti, M. G. Bellino, P. Innocenzi, and G. J. A. A. Soler-Illia, Chem. Mater. **21**, 2763 (2009).
[81] G. L. Drisko, A. Zelcer, V. Luca, R. A. Caruso, and G. J. A. A. Soler-Illia, Chem. Mater. **22**, 4379 (2010).
[82] Experiments also show that the evaporation of single solvent can only fabricate homogeneous mesopores [80,81] with the pore size equal to that of small pores from the evaporation of binary solvents. These small pores observed in experiments [80,81] are caused by the self-assembly of surfactants and transition-metal precursors during the evaporation process.